Available online at www.sciencedirect.com
SCIENCE DIRECT
Biochimica et Biophysica Acta 1757 (2006) 240–252
BIOCHIMICA ET BIOPHYSICA ACTA
BBA
http://www.elsevier.com/locate/bba

Reduction of nitric oxide in bacterial nitric oxide reductase—a theoretical model study

L. Mattias Blomberg *, Margareta R.A. Blomberg, Per E.M. Siegbahn

Department of Physics, Stockholm University, SE-106 91 Stockholm, Sweden

Received 5 February 2006; received in revised form 7 April 2006; accepted 7 April 2006
Available online 21 April 2006

Abstract

The mechanism of the nitric oxide reduction in a bacterial nitric oxide reductase (NOR) has been investigated in two model systems of the heme-b_3-Fe_B active site using density functional theory (B3LYP). A model with an octahedral coordination of the non-heme Fe_B consisting of three histidines, one glutamate and one water molecule gave an energetically feasible reaction mechanism. A tetrahedral coordination of the non-heme iron, corresponding to the one of Cu_B in cytochrome oxidase, gave several very high barriers which makes this type of coordination unlikely. The first nitric oxide coordinates to heme b_3 and is partly reduced to a more nitroxyl anion character, which activates it toward an attack from the second NO. The product in this reaction step is a hyponitrite dianion coordinating in between the two irons. Cleaving an N − O bond in this intermediate forms an Fe_B (IV)═O and nitrous oxide, and this is the rate determining step in the reaction mechanism. In the model with an octahedral coordination of Fe_B the intrinsic barrier of this step is 16.3 kcal/mol, which is in good agreement with the experimental value of 15.9 kcal/mol. However, the total barrier is 21.3 kcal/mol, mainly due to the endergonic reduction of heme b_3 taken from experimental reduction potentials. After nitrous oxide has left the active site the ferrylic Fe_B will form a μ-oxo bridge to heme b_3 in a reaction step exergonic by 45.3 kcal/mol. The formation of a quite stable μ-oxo bridge between heme b_3 and Fe_B is in agreement with this intermediate being the experimentally observed resting state in oxidized NOR. The formation of a ferrylic non-heme Fe_B in the proposed reaction mechanism could be one reason for having an iron as the non-heme metal ion in NOR instead of a Cu as in cytochrome oxidase.

Keywords: Nitric oxide reductase; NOR; Heme-copper oxidase; Nitrous oxide; Nitric oxide; DFT; B3LYP

1. Introduction

The respiratory bacterial nitric oxide reductase catalyzes the reduction of two nitric oxides to nitrous oxide and water according to Eq. (1).

$$2NO + 2e^- + 2H^+ \rightarrow N_2O + H_2O \quad (1)$$

NO reduction is a part of the bacterial denitrification process reducing nitrate to di-nitrogen in four steps ($NO_3^- \rightarrow NO_2^- \rightarrow NO \rightarrow N_2O \rightarrow N_2$), catalyzed by nitrate reductase (NAR), nitrite reductase (NIR), nitric oxide reductase (NOR) and nitrous oxide reductase (NOS), respectively. Denitrification is the anaerobic counterpart to mitochondrial and bacterial respiration, driven by the reductants formed in the metabolism and generating an electro chemical gradient used to synthesize ATP. The enzyme catalyzing the formation of the N − N bond in denitrification is nitric oxide reductase.

Respiratory bacterial NOR is biochemically distinct from the flavorubredoxin cytoplasmic nitric oxide reductase [1] and the P450 NORs in fungal denitrification [2]. The most studied bacterial respiratory nitric oxide reductases belong to the NorCB class of enzymes purified from *Paracoccus denitrificans, Pseudomonas stutzeri* and *Paracoccus Halodenitrificans* [3–7]. The smaller NorC subunit is a membrane bound cytochrome *c*, proposed to be the site of electron entry corresponding to Cu_A in cytochrome *c* oxidase. The larger catalytic NorB subunit is suggested to consist of 12 transmembrane α-helices containing the bis-histidine coordinated low spin heme *b* and the magnetically coupled binuclear center consisting of a high spin heme b_3 and a high spin non-heme iron [3,8] corresponding to heme *a* and heme a_3-Cu_B in cytochrome *c* oxidase.

* Corresponding author.
E-mail address: mattiasb@physto.se (L.M. Blomberg).

0005-2728/$ - see front matter © 2006 Elsevier B.V. All rights reserved.
doi:10.1016/j.bbabio.2006.04.008

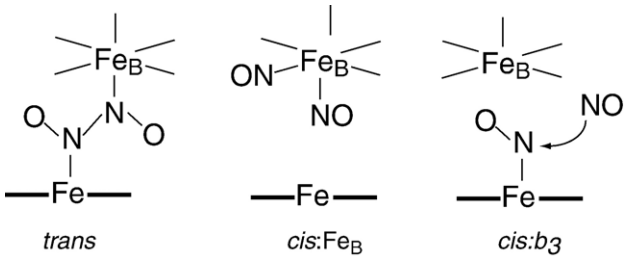

Fig. 1. Proposed mechanisms for NO reduction in respiratory nitric oxide reductase.

The tertiary structures of the catalytic subunit NorB and the corresponding subunit I in cytochrome oxidases are believed to be very similar [9]. The sequence homology in the two enzyme families is significant, and all six metal binding histidines are conserved. Several structures of cytochrome oxidases have been determined of which the ba_3-type oxidase of *Thermus thermophilus* and bo_3-type oxidase of *Escherichia coli* have been shown to reduce NO. In contrast, no structure has to date been determined for a respiratory nitric oxide reductase. However, Zumft et al. have used the crystal structure of cytochrome *c* oxidase from *Pa. denitrificans* to generate a model of NorB from the primary sequence in *P. stutzeri* [9]. In this model the α-helices of NorB are almost superimposable with the oxidase structure's, and the conserved histidines coordinating the heme *b* (His60 and His349), heme b_3 (His347) and Fe_B (His207,258–259) are positioned at the corresponding residues in cytochrome *c* oxidase. Mutagenesis of His258 have shown that it is necessary for the activity of the enzyme [10], which implies that it probably is a ligand to the non-heme iron. In addition to the three histidines, Glu211 (198 in *Pa. denitrificans*), which is conserved in NOR, has been shown to be essential for the activity by site-directed mutation in *Pa. denitrificans* [11]. Glu211 is located approximately one turn below His207 in α-helix IV, and has been proposed to be a ligand to Fe_B or to be involved in the protonation steps during the catalysis. However, in the modeled structure, both the conserved Glu211 and Glu280 are too far away to coordinate to Fe_B and are instead hydrogen bonding to His207 and His258, respectively [9].

In contrast to oxidases the protons consumed in the reduction of nitric oxide are taken from the periplasmic side of the membrane and NOR is thus nonelectrogenic [12]. Furthermore, heme b_3 has been shown to have an unusually low reduction potential and NOR has been proposed to be three electron reduced at physiological conditions, with heme b_3 remaining oxidized [5]. One reason proposed for keeping heme b_3 oxidized is to avoid the formation of a too stable ferrous nitrosyl complex, which may inhibit the enzyme. A five coordinated heme b_3 in a μ-oxo bridged Fe(III)–O–Fe_B (III) species has been characterized as the resting state in the oxidized NOR and has been proposed to be an intermediate during turnover [13].

Several mechanisms (Fig. 1) have been proposed for the NO reduction such as the *cis* mechanism where both NOs are bound to one of the metal centers and the *trans* mechanism where one NO is bound to each one of the metal centers. In the *cis:*b_3 mechanisms, a second NO attacks the nitrogen atom of a nitric oxide coordinated to heme b_3.

In the present study, the mechanism of nitric oxide reduction has been investigated for two models of the binuclear center. The models differ in the coordination of the non-heme Fe_B where model A has an octahedral coordination incorporating Glu211 (198) in the first shell together with a water molecule in addition to the three histidines. Model B on the other hand has a tetrahedral

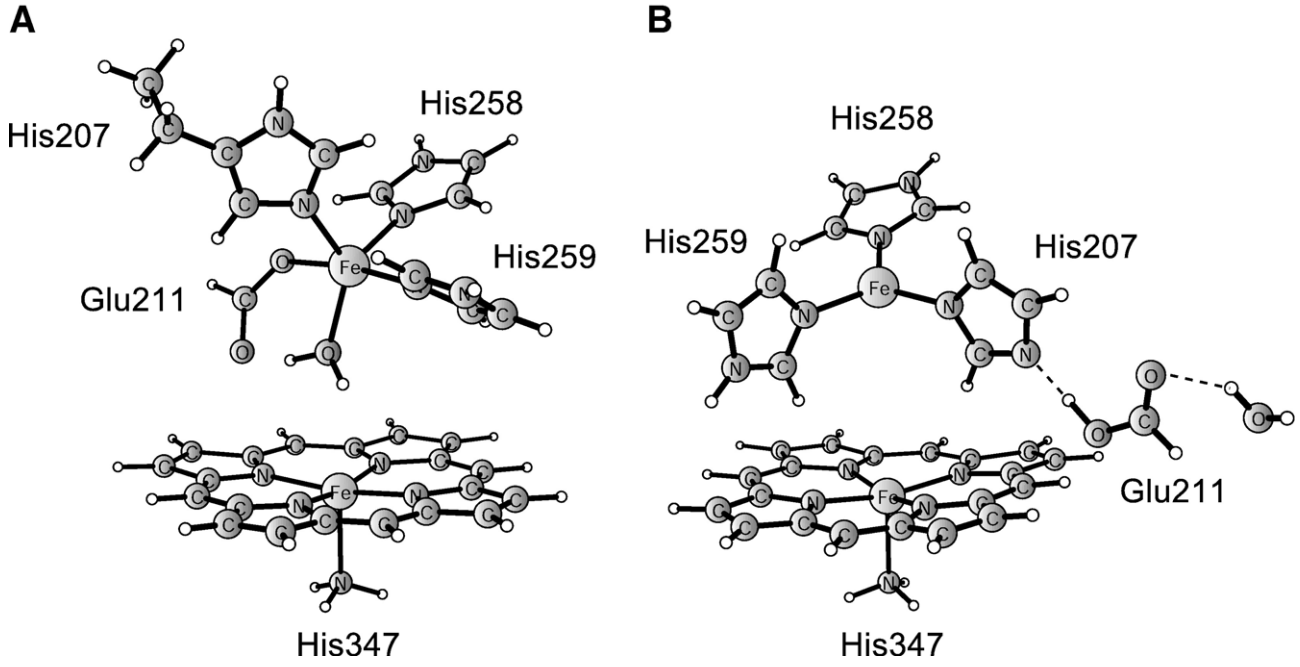

Fig. 2. The numbering of the histidine and glutamate residues is taken from *P. stutzeri*, but is arbitrary since the structure has not been determined. Models A and B of the binuclear center in NOR.

coordination binding the three conserved histidines whereas the glutamate is located in the second shell, hydrogen bonding to one of the histidines. Model A and B (Fig. 2) are further described below in Section 2. Free energy profiles for NO reduction have been constructed for both models and the energetics gives important information on the mechanism of nitric oxide reduction. The present study do not intend to prove the coordination sphere of Fe_B , but rather to find out what features of the non-heme Fe_B are important for the binuclear center to be able to reduce nitric oxide and which type of mechanism is favored.

2. Models

The structure of nitric oxide reductase has not been determined to date. However, as discussed above the primary sequence of NorB in *P. stutzeri* have been fitted to the crystal structure of the cytochrome *c* oxidase in *Pa. denitrificans*, generating a model of NorB [9]. In the NorB model the three histidines conserved in all heme-copper oxidases are positioned as ligands to the non-heme iron (Fe_B). In the second shell, Glu211 conserved in NOR, and Glu280 are hydrogen bonding to the first shell ligands. In contrast to the model of NorB, a very common coordination of mononuclear non-heme iron is the 2-His–1-Glu/Asp motif [14] with the remaining sites filled by water forming an octahedral coordination. Furthermore, there are other coordination motifs for mononuclear non-heme iron enzymes incorporating tyrosines, glutamine/asparagine, histidine, glutamate/aspartate [15]. Recently the structure of a flavodiiron protein from *Moorella thermoacetica* showing nitric oxide reductase activity was determined [16,17]. In this enzyme, the diiron site is ligated by four histidine, two aspartates and one glutamate. Common for these different non-heme iron coordinations are a mixture of nitrogen and oxygen based ligands forming an octahedral coordination sphere around the iron. This structural information from the non-heme irons in other systems implies that a tetrahedral coordination by three histidines in the model of NorB is rather unlikely.

In the present study, the two models shown in Fig. 2 have been investigated. Model A has an octahedral coordination, incorporating Glu211 and a water molecule in addition to the three conserved histidines. This model is constructed on the basis of the suggested Fe_B ligands and the common coordination motifs generally found in non-heme iron enzymes. Model B on the other hand corresponds to the model of NorB discussed above, which is the only three-dimensional structural information for a respiratory nitric oxide reductase. In model B, the three histidines are coordinating to the non-heme iron and one glutamate is hydrogen bonding to one of the histidines as a second shell ligand.

In Model A Glu211, His207, His258, His259 and a water molecule are ligands to the non- heme iron, making the coordination of Fe_B octahedral. The histidine *trans* to the empty site of Fe_B (Fig. 2) is modeled as a 4-ethylimidazole, whereas the two remaining histidines coordinating to the non-heme iron are modeled as unsubstituted imidazoles. The larger model of the histidine sitting *trans* to the binding site on Fe_B was used at an early stage in the present study. Since many of the intermediates were already optimized with this model, it was used throughout the study. The differences in the models of the histidines will not affect the results. The glutamate is modeled as a formate ion, heme b_3 as a porphyrin ring without substituents and the proximal histidine (His347) as ammonia, which is a well tested model of histidines coordinated to hemes.

In model B, heme b_3 is modeled identically to model A described above. The three histidines coordinating to Fe_B are modeled as imidazoles. The glutamate, modeled as formate, and the water coordinating directly to the non-heme iron in model A are located in the second shell in model B, see Fig. 2. The glutamate is hydrogen bonding to His207 and in addition the water molecule is forming a hydrogen bond to the other oxygen of the glutamate, which is important in the calculations to avoid spin appearing on this oxygen. Furthermore, it is possible that the glutamate would form a hydrogen bond to a polar residue or peptide bond in the enzyme.

The two models have the same ligands and charge which should make them comparable. In Section 4, the catalytic mechanism and the energetics of these two models will be discussed.

3. Methods

The geometries of the stationary points involved in the reaction studied were optimized using Becke's [18] three parameter hybrid exchange functional combined with the Lee–Yang–Parr [19] correlation functional (B3LYP). The calculations were performed using the GAUSSIAN-03 [20] and JAGUAR [21] programs. The geometries were optimized with the double-ζ quality basis set lacvp implemented in JAGUAR [21] with an effective core potential (ECP) on iron. Most intermediates are open shell systems, which were treated using unrestricted B3LYP.

The normal procedure in a theoretical investigation of a reaction mechanism catalyzed by an enzyme, is to cut out the important residues of the active site and freeze one of the coordinates of each residue, for example the β-carbons, according to the crystal structure. The freezing is done to model the restriction imposed on the residues by the protein matrix. However, in the present study no structure has been determined, and thus most of the calculations are made without restrictions. There are a few exceptions where restrictions had to be made such as for the heme-b_3–Fe(III)–Fe_B (II) intermediate where the metal centers drifted apart during the optimization. Therefore, the hydrogens corresponding to β-carbons of the Fe_B ligands and the nitrogen of the proximal histidine to heme b_3 were restricted in the heme-b_3–Fe(III)–Fe_B (II) and heme-b_3–Fe(II)–Fe_B (II) intermediates. The latter intermediate was also fully optimized to connect the restricted model to the unrestricted to be able to compare the energetics.

The entropy effect is estimated to be 10 kcal/mol when a di- or tri-atomic molecule is bound or released [22,23]. Furthermore, it has been shown for similar reactions that the entropy cost in the transition state when binding di- and triatomic molecules is very close to the total entropy cost of forming the bond [22,23]. Because the entropy effects have not been calculated, the same entropy correction is used for both transition and bound states.

The final energies for the optimized geometries were evaluated using the lacv3p**+basis set of JAGUAR, which is a triple-zeta basis set with an ECP on the irons and including one diffuse function on all heavy atoms and one polarization function on first and second row atoms. The dielectric effects from the surroundings were obtained for all stationary points using the Jaguar self-consistent reaction field method [24] using the lacvp basis set. The dielectric constant was set equal to 4 [25]. The probe radius of the solvent was set to 1.4 Å, which corresponds to the radius of a water molecule.

Describing the surrounding protein matrix as a dielectric continuum is a rather crude model especially when calculating electron and proton affinities. The importance of including effects of explicit charges and inhomogeneities of the protein on pK_a values has been emphasized [26]. In that study the protonation sites were located at the surface of the quantum chemical model. However, in the present study, the positions of the protonation of different intermediates are located in between the two metal ions and the most important interactions are thus described by the quantum chemical model. Furthermore,

the total charge of the model is the same for all calculated electron (+2) and proton affinities (+1), respectively. By comparing intermediates where the total charge is equal and the most important interactions are described by the quantum chemical model, the effects of the surrounding protein should be similar.

The accuracy of the B3LYP functional has been tested in the extended G3 benchmark set [27], which consists of enthalpies of formation, ionization potentials, electron affinities and proton affinities for molecules containing first- and second-row atoms. The B3LYP functional gives an average error of 4.3 kcal/mol [27] for 376 different entries. Due to the lack of accurate experimental data for transition metals, there are few benchmark tests. Normal metal–ligand bond strengths indicate that the errors are in the range, 3–5 kcal/mol [28]. Different aspects of modeling enzyme active sites have been reviewed [29,30].

4. Results and discussion

In the present section, the reaction steps in the reduction of nitric oxide to nitrous oxide and water in two models of the active site of NOR are discussed. The models, A and B, have been described above in Section 2 and are shown in Fig. 2. During the reaction two electrons and two protons are transferred to the binuclear site (Eq. (1)). The energetics for the proton and electron transfers, obtained by a combination of calculated proton and electron affinities and experimental data, are considered below in Section 4.1. The calculated energetics for the formation of the N − N bond, and the cleaving of an N − O bond forming nitrous oxide and water are combined with the estimated thermodynamics of the electron and proton transfers to create energy profiles for the whole catalytic cycle, which are discussed below in Sections 4.2 (model A) and 4.3 (model B).

The lack of structural information for NOR makes the models used in the present study more hypothetical than in other mechanistic studies such as the reduction of NO in a *ba*$_3$- type of cytochrome oxidase investigated in a previous study [32]. Consequently, the energetics obtained contains larger uncertainties than usual. However, as mentioned above the present study does not intend to determine the coordination of the non-heme Fe_B, but rather increase the understanding of what is necessary for the binuclear center to catalyze the reduction of NO, and furthermore to give some insight into which mechanism is used. Thus, the significance of small energy changes in the free energy profiles obtained below should not be over-interpreted.

4.1. Energetics of the proton and electron transfers

The energetics of the electron and proton transfers can in principle be obtained as the difference in electron affinities (EA), and proton affinities (PA), respectively, between an acceptor and a donor. However, the energetics of these charge transfer reactions are difficult to estimate accurately, since the calculated values are sensitive to the surroundings, and thus to the model used. However, relative values within the same model are generally much more accurate. The energies of the proton and electron transfers are needed to create energy profiles for the catalytic cycles, and are thus of importance for the overall picture of the reaction mechanism. How the experimental reduction potentials can be used when the energetics of the electron and proton transfers in the reduction process (Eq. (1)) is estimated, is described below.

The midpoint reduction potentials (E_m) for heme *c*, *b*, b_3 and Fe_B in *Paracoccus denitrificans* are known from experiments, and are 310, 345, 60 and 320 mV [5], respectively. In the models of NOR used in the present study heme b_3 and Fe_B are incorporated, for which the electron affinities can be calculated. Since the structure of heme b_3 is identical in the two models, and also much better characterized experimentally, as compared to Fe_B, the reduction of heme b_3 is chosen as a reference. According to the experimental reduction potentials given above, an electron transfer from a ferrous heme *b* to a ferric heme b_3 is endergonic by 6.6 kcal/mol. Thus, the electron affinity of heme *b* is set to be 6.6 kcal/mol higher than the calculated electron affinity of heme b_3. The EA of heme *b* can then be used to evaluate the energetics of the second electron transfer during the reduction of NO. The reference EA of heme *b* will differ between models A and B due to the different coordinations of Fe_B.

The calculated electron affinity (EA) of heme-b_3–Fe(III) Fe_B (II) in model A is 114.5 kcal/mol. Thus, the electron affinity of the ferric heme *b* was parametrized to be $EA^A_{\text{heme b}}$=121.1 kcal/mol. The corresponding EA in model B is 120.9 kcal/mol and heme *b* would in this case have an $EA^B_{\text{heme b}}$=127.5 kcal/mol.

Furthermore, it is known that the potential for the reduction of two nitric oxides to nitrous oxide and water according to Eq. (1) is E'_0 (pH=7.0)=1.177 V (SHE), which corresponds to a $\Delta G'_0$=−54.3 kcal/mol. In the present study, the electrons are taken from heme *b* which has a reduction potential of 345 mV [5]. The reduction potential for Eq. (1) can thus be transferred from the standard hydrogen electrode (SHE) reference to heme *b*, which gives a $\Delta G''_0$=−38.4 kcal/mol for the overall reaction. Thus, both the energetics of the two electron transfers from heme *b* and the overall energy of the reaction can be estimated.

To complete the picture, the energy cost for bringing two protons from the bulk (pH=7) to the binuclear center has to be determined. The proton affinities for the intermediates abstracting a proton can be calculated. Since the energetics of the two electron transfers are known, the energetics of the two proton transfers can be parametrized to fit the overall energy of the reaction. In this way, a reference value for the PA of the bulk at pH=7 can be obtained. Similar to the electron affinities discussed above, the reference PA of the bulk will differ between models A and B due to the different coordination of Fe_B. The proton affinity of the bulk was in this way parametrized to be PA^A_{bulk}=273.5 and PA^B_{bulk}=264.8 kcal/mol in model A and B, respectively.

To compare the calculated energetics with the reduction potential determined according to the standard state of the reactants and products, the gas phase energies are used for NO and N_2O. Furthermore, the ΔG_{solv} for water is taken from experiments.

In Sections 4.2 and 4.3 below, free energy profiles for model A and B (Fig. 2) are constructed, including the energetics of the electron and proton transfers obtained as described above. The dashed barriers in the energy profiles presented below correspond to the barriers of the proton transfers which have not been calculated. Furthermore, the barriers for the leaving of the neutral products N_2O and H_2O are dashed. These barriers are expected to be low since the processes are either exergonic and/or the oxidation states of the metal ions are unaltered.

4.2. Model A

In model A the non-heme Fe_B has an octahedral coordination, see Fig. 2. The resulting free energy profile of the reduction of NO is shown in Fig. 3.

4.2.1. Binding of NO

In the reduced form of NOR heme *c*, heme *b* and the non-heme Fe_B are in their ferrous states, whereas heme b_3 has an unusually low reduction potential, and is proposed to remain in a ferric state [5]. The first step in the reaction is to bind nitric oxide. The bond strength to the mixed valence heme-b_3–Fe(III) Fe_B (II) binuclear site is low but increases if the active site is fully reduced (heme-b_3–Fe(II)–Fe_B (II)). NO has been shown to coordinate to heme b_3 in the fully oxidized NOR in a resonance Raman spectroscopy study [32]. In the calculations it is difficult to evaluate if NO first binds to the ferric heme b_3, which would increase the reduction potential of the latter substantially, probably inducing the reduction, or if the electron has to be transferred before NO can bind. The free energy of binding NO to the ferrous heme is −3.1 kcal/mol. Relative to the resting ferric heme b_3 NO is unbound by 3.5 kcal/mol, see Fig. 3.

The bond strength between ferrous heme iron and diatomic molecules, and particularly the bond strength of NO, has been shown to be underestimated using the B3LYP functional. The calculated bond strength of NO in cytochrome oxidase was underestimated by 7–8 kcal/mol [33]. If the bond strength of NO to the ferrous heme b_3 in NOR was corrected by 7 kcal/mol, NO would be bound by 3.5 kcal/mol relative to the mixed valence binuclear center, and nitric oxide bound to the fully reduced binuclear center would be the resting state. NO has also been proposed to bind to the non-heme iron but with the coordination of model A NO prefers to bind to the heme iron by 4.3 kcal/mol. The trend of NO binding stronger to the heme is not very sensitive to the particular ligands coordinating to the non-heme iron. Several models of Fe_B with different octahedral coordination show a preference for binding NO to the ferrous heme iron (data not shown). The endergonic reduction of heme b_3 is chosen to be the first step in the reaction mechanism in the present study, which might seem unfavorable, but regarding the increase in affinity for NO by the ferrous heme makes it reasonable. The order of these two steps could be altered, but the energy difference between the mixed valence and the fully reduced binuclear center binding NO is the same. However, both k_{on} and the affinity for NO should decrease compared to having a reduced heme as the resting state.

In an EPR study, the proximal histidine has been shown to leave its coordination to heme b_3 when nitric oxide binds to the ferrous heme [34]. In the calculations, on the other hand, the proximal histidine is bound to the heme by around 8 kcal/mol. The endergonicity of expelling the proximal histidine could be counterbalanced to some extent by the formation of a hydrogen bond to a polar residue or alternatively to a peptide, which is not included in the model. Since the proximal histidine is bound to heme b_3 according to the calculations, the coordination is kept. Heme b_3 being five or sixth coordinated should have only small effects on the energetics of the investigated reduction mechanism.

The binding of NO oxidizes the ferrous high spin heme-b_3 to a low spin heme in between Fe(II) and Fe(III) with a spin population of 0.40. Consequently, NO is partly reduced to a more nitroxyl anion character, antiferromagnetically coupled to Fe_B and the slightly oxidized heme b_3. The spin population on N1 and

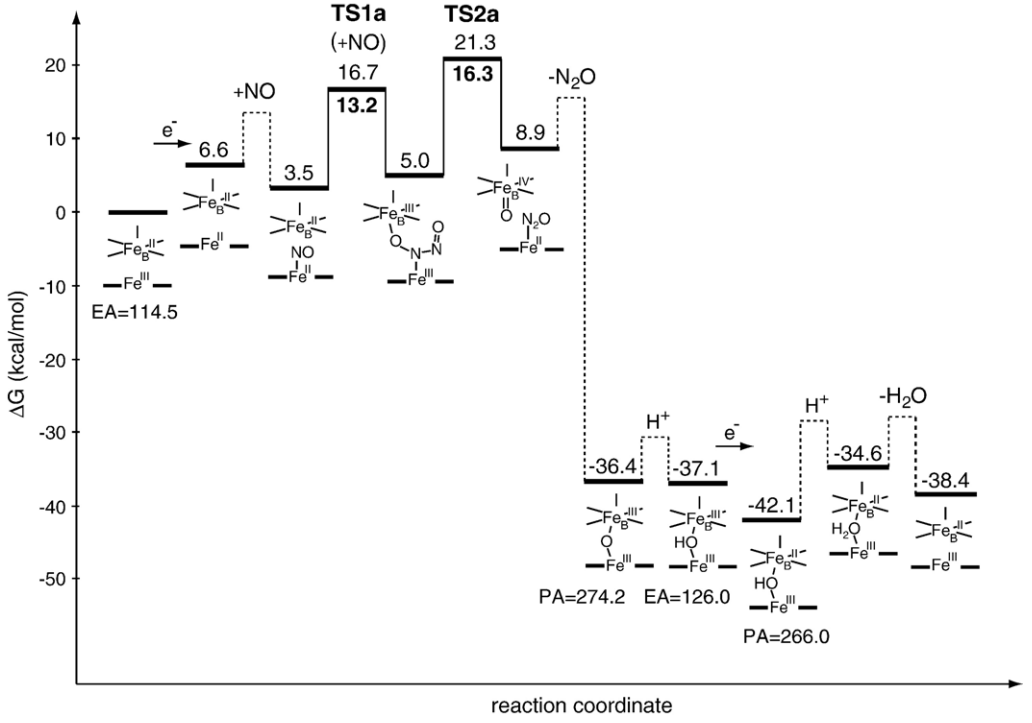

Fig. 3. Free energy profile of model A, octahedral Fe_B.

O2 is −0.84 and −0.47, respectively. Fe_B stays ferrous high spin with a spin population of 3.83, see Fig. 4 for bond distances and spin populations.

4.2.2. Formation of the N−N bond

The nitroxyl anion ($^3NO^-$) is known to react very fast with nitric oxide in solution [35], whereas two nitric oxide molecules cannot form a stable covalent bond. Thus, NO being partly reduced by coordinating to heme b_3 should activate it toward the attack by the second NO. The barrier of TS1a is 13.2 kcal/mol, relative to the nitrosyl intermediate, including an assumed entropy cost for bringing NO to the transition state of 10 kcal/mol, see Fig. 3. The large entropy contribution to TS1a makes the barrier somewhat uncertain and dependent on the concentration of NO. Thus, 13.2 kcal/mol can be regarded as the maximum barrier height for this reaction step. The total barrier of TS1a compared to the empty mixed valence binuclear center is 16.7 kcal/mol. However, regarding the assumed underestimation of the Fe−NO bond strength discussed above, the nitrosyl intermediate should be the resting state and the total barrier would then be 13.2 kcal/mol. It should be noted that there is a spin flip of NO coordinated between the two irons on approaching TS1a, resulting in an antiferromagnetic coupling between heme b_3 and Fe_B , and a ferromagnetic coupling between NO and Fe_B . The change in spin stabilizes the hyponitrite dianion intermediate formed. In the transition state the N–N distance is 2.20 Å and heme b_3 is slightly more oxidized compared to the heme b_3 nitrosyl intermediate, the former having a spin population of −0.49. Fe_B stays in a ferrous state with a spin population of 3.85. The two nitric oxides have opposite spins with a spin population of 0.65 on the nitrogen coordinated to the heme (N1) and −0.48 on the second NO's nitrogen (N3). The oxygen of the coordinated nitric oxide (O2) and the oxygen (O4) of the second NO have spin populations 0.38 and −0.16, respectively. The decrease in the spin population on the second NO shows that an N−N bond starts to form, see Fig. 5 for distances and spin populations.

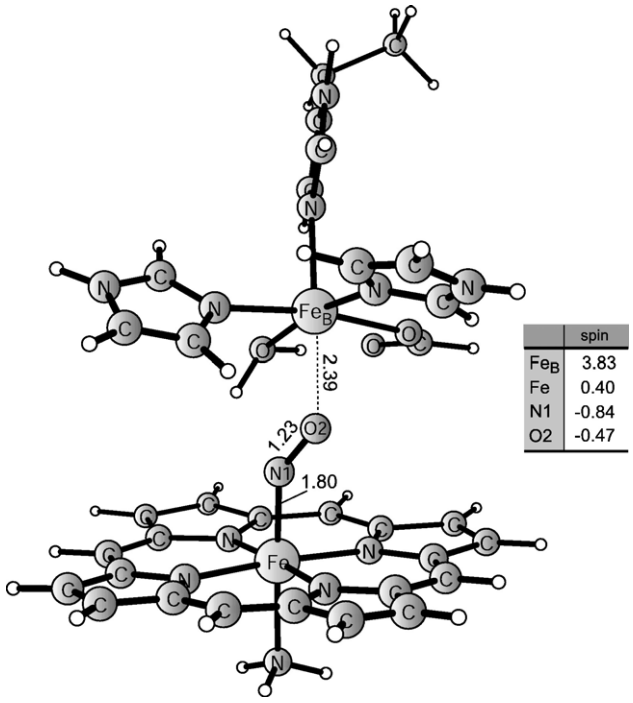

Fig. 4. Nitric oxide coordinating to the ferrous heme b_3.

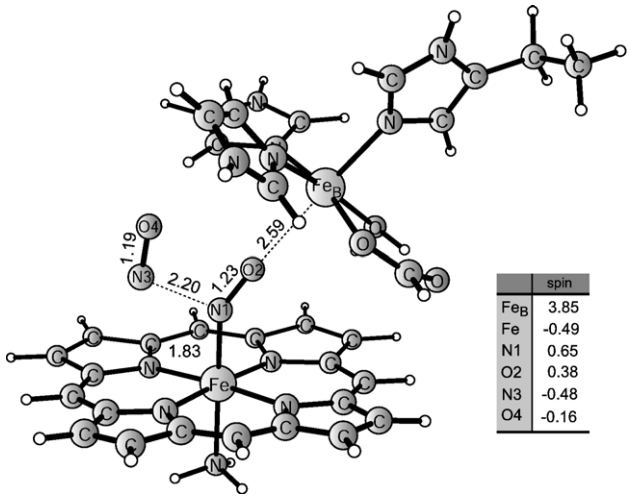

Fig. 5. TS1a, a second nitric oxide attacks the one coordinating to the ferrous heme b_3.

After the N−N bond is formed both irons are in their ferric state with a spin population of −1.03 and 4.04 on the heme b_3 and Fe_B, respectively. The structure of $N_2O_2^{2-}$ corresponds to an isomer of hyponitrous acid where the protons are replaced by the metal ions stabilizing it in a similar way, see Fig. 6 for bond lengths and spin populations. In principle, the hyponitrite dianion intermediate, $N_2O_2^{2-}$, should be a closed shell species. However, most of the spin on this intermediate is located on O2 and can be regarded as a spin delocalization from the ferric Fe_B. The reaction step is endergonic by 1.5 kcal/mol compared to the nitrosyl intermediate and a free nitric oxide, see Fig. 3.

4.2.3. Cleaving an N−O bond forming N_2O

To form nitrous oxide one N−O bond in the hyponitrite dianion intermediate (Fig. 6) has to be cleaved. The transition state of this reaction step is shown in Fig. 7. The N−O bond length has increased to 2.30 Å while the Fe_B−O bond length has decreased to 1.74 Å. In the transition state an electron is transferred from the non-heme iron to heme b_3 forming a ferrylic non-heme Fe_B and N_2O coordinating to a ferrous heme b_3. The energy cost of forming the high valent non-heme Fe_B (IV)═O is compensated by the formation of a stable N_2O giving a reaction step endergonic by only 3.9 kcal/mol compared to the preceding intermediate, see Fig. 3. The reaction mechanism described above corresponds to the so-called *cis*:b_3 mechanism discussed in Section 1. Other possible mechanisms for the NO reduction are discussed below in Section 4.2.5.

The ferrylic Fe_B and O3 have spin populations of 3.12 and 0.70, respectively, which are typical spin population for a non-heme Fe (IV)═O intermediate [36,37]. The Fe–O2 bond length is 1.65 Å which also is a typical feature of a ferrylic iron. The intrinsic barrier for cleaving the N−O bond is 16.3 kcal/mol. However, the resting state in Fig. 3 is the mixed valence binuclear center, which makes

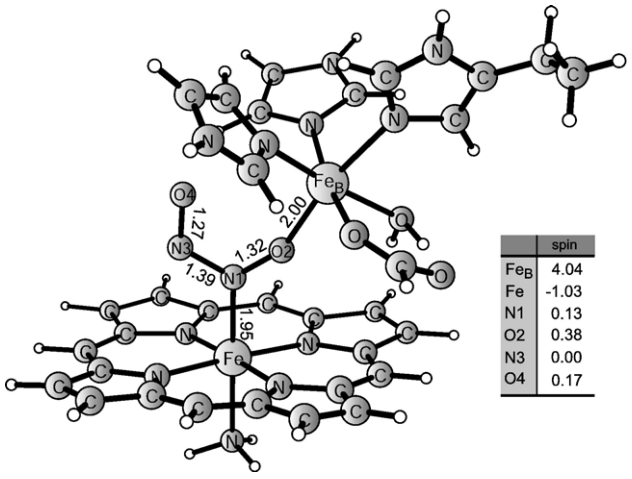

Fig. 6. The hyponitrite dianion intermediate coordinating between a ferric heme-b_3 and Fe_B.

the total barrier 21.3 kcal/mol. The turnover rate in NOR (*P. denitrificans*) is ~ 1400 mol NO mol enz^{-1} min^{-1} [38], which corresponds to a barrier of 15.9 kcal/mol. Thus, the intrinsic barrier of TS2a is very close to the experimental barrier, but the slightly endergonic steps leading to the formation of the hyponitrite dianion intermediate adds to this barrier and makes it around 5 kcal/mol too high. However, considering the uncertainties in the model used in the present study the agreement is satisfactory.

The ferrylic Fe_B and ferrous heme b_3 coordinating nitrous oxide is an unstable intermediate. By expelling N_2O, a μ-oxo bridge can be formed between the two ferric irons, which is exergonic by 41.4 kcal/mol compared to the hyponitrite dianion intermediate. The μ-oxo bridged binuclear center has been characterized spectroscopically as a five coordinated high spin species antiferromagnetically coupled to the high spin Fe_B [4,13], which is interpreted as heme b_3 being five coordinated. Heme b_3 has been shown to become five coordinated already when NO binds, as discussed in Section 4.2.1. In the calculations, the proximal histidine is coordinating to a low spin heme in the μ-oxo bridged structure (Fig. 8). By removing the proximal histidine the high spin heme becomes energetically favored in agreement with experiments. However, in the calculations, the bond strength to the proximal histidine is around 15 kcal/mol. As discussed in Section 4.2.1, the endergonicity of expelling the proximal histidine could to some extent be counterbalanced by the formation of a hydrogen bond between the histidine and a polar residue or a peptide, which is not included in the model. The thermodynamics of the expulsion of the sixth ligand cannot be explained by calculations on the present model, and the proximal histidine is therefore remaining coordinated to heme b_3 throughout the reaction sequence.

4.2.4. Reduction of the μ-oxo bridge to water

To return to the starting point in the catalytic cycle the μ-oxo bridged diferric binuclear site has to be protonated and reduced. In Section 4.1, the electron and proton affinities were parametrized to experimental reduction potentials giving an $EA^{A}_{heme\ b}$=121.1 kcal/mol and PA^{A}_{bulk}=273.5 kcal/mol, respectively. Using these reference values together with the calculated proton and electron affinities of the different intermediates gives an essentially thermoneutral free energy profile of the remaining reaction steps, see Fig. 3.

Experimentally the resting state of the oxidized NOR has been proposed to be an unprotonated μ-oxo bridge between heme b_3 and Fe_B [13,39,40]. This is not in perfect agreement with the calculations where the protonation of the μ-oxo bridge is approximately thermoneutral, but it is within the uncertainty of the method used. From experimental reduction potentials for Fe_B measured at different pH, the formation of a hydroxyl group or water in between the ferric heme b_3 and ferrous Fe_B can be calculated to be endergonic by 2.4 (OH) and 0.5 (H_2O) kcal/mol relative to the μ-oxo bridge, respectively [5,40]. In the calculations, the corresponding reactions are exergonic by 5.7 and endergonic by 1.8 kcal/mol (Fig. 3), respectively, in reasonable

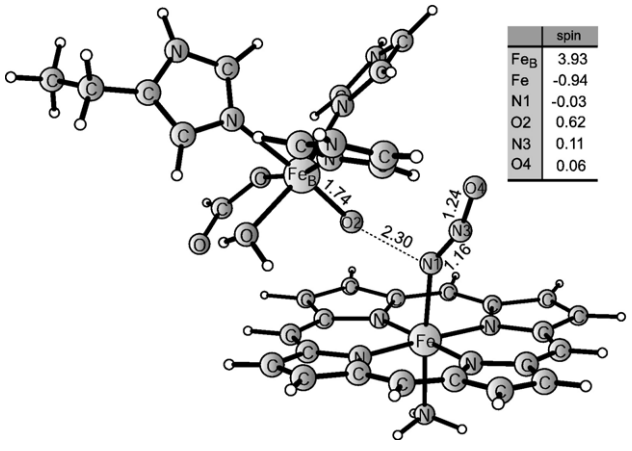

Fig. 7. TS2a, cleaving the N – O bond forming a ferrylic Fe_B and nitrous oxide coordinating to a ferrous heme b_3.

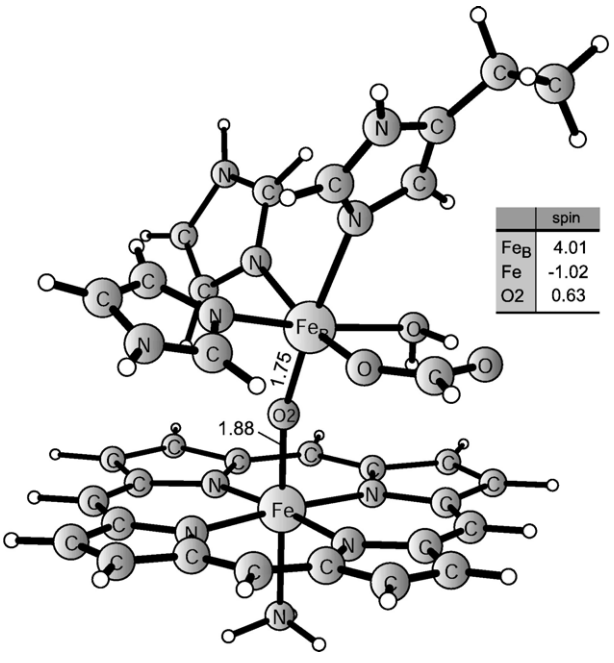

Fig. 8. Ferric heme b_3 and Fe_B bridged by a α-oxo group. oxo-bridged diferric binuclear center, model A.

agreement with the experiments. The calculated exergonicity of the formation of the hydroxyl group bridging the ferric heme b_3 and ferrous Fe_B would affect the rate determining barrier in the next catalytic cycle. However, according to the experimental reduction potentials discussed above, this reaction step is endergonic, and therefore this intermediate is not considered as the resting state in the next cycle. It should be noted that the pH used measuring the reduction potentials forming OH and H_2O are 6 and 8.5, respectively, whereas the pH in the calculations is parameterized to be 7. However, in terms of free energy, these differences in pH affect the reduction processes only slightly (1–2 kcal/mol), decreasing the difference between the calculated and experimental results.

The full free energy profile for the reduction of nitric oxide to nitrous oxide and water in model A is summarized in Fig. 3. The energetics obtained with model A, having an octahedral coordination of Fe_B, is feasible and in satisfactory agreement with experiments. In Section 4.3, below, the corresponding mechanism with model B is discussed.

4.2.5. Alternative mechanisms

As mentioned above, several mechanisms (Fig. 1) have been proposed for the NO reduction. The main mechanisms are the *cis* mechanism where both NOs are bound to the same metal ion, and the *trans* mechanism where the two NOs are bound to different metal centers. The reaction mechanism described above corresponds to the so-called *cis:b*$_3$ mechanism where a second NO attacks the nitrogen atom of a nitric oxide coordinated to heme b_3.

Forming the corresponding *trans* structure of the hyponitrite dianion with the two nitrogens coordinated to different irons is 0.5 kcal/mol more stable compared to the *cis:b*$_3$ structure (Fig. 6). Thus, when the second NO enters the active site, there will be a competition between binding to the non-heme Fe_B and reacting with the already activated NO coordinating to heme b_3. The forward reaction of the *trans* type of structure would have to be protonation and reduction until O2 can be released as water. The proton affinity (PA) of the *trans* hyponitrite dianion is quite low leading to a proton transfer endergonic by 14.3 kcal/mol. The following electron transfer is exergonic by 9.5 kcal/mol, which makes the reduction of the hyponitrite dianion to hyponitrite energetically possible. However, the second protonation of O2 is very endergonic and forces the N – O bond to cleave forming H_2O and N_2O in a very exergonic reaction step. During the optimization of the intermediate with a doubly protonated O2 a semi stable structure was obtained before the N – O bond broke spontaneously. This doubly protonated intermediate is >30 kcal/mol higher in energy than the hyponitrite intermediate. Thus, the very low proton affinity of the hyponitrite will most likely make the barrier for the protonation and the N – O bond cleavage too high. If the reaction would occur it would go through a concerted type of mechanism. The energetics of this type of mechanism cannot be evaluated with the present model since the residue from which the proton would be taken has to be included in the model,

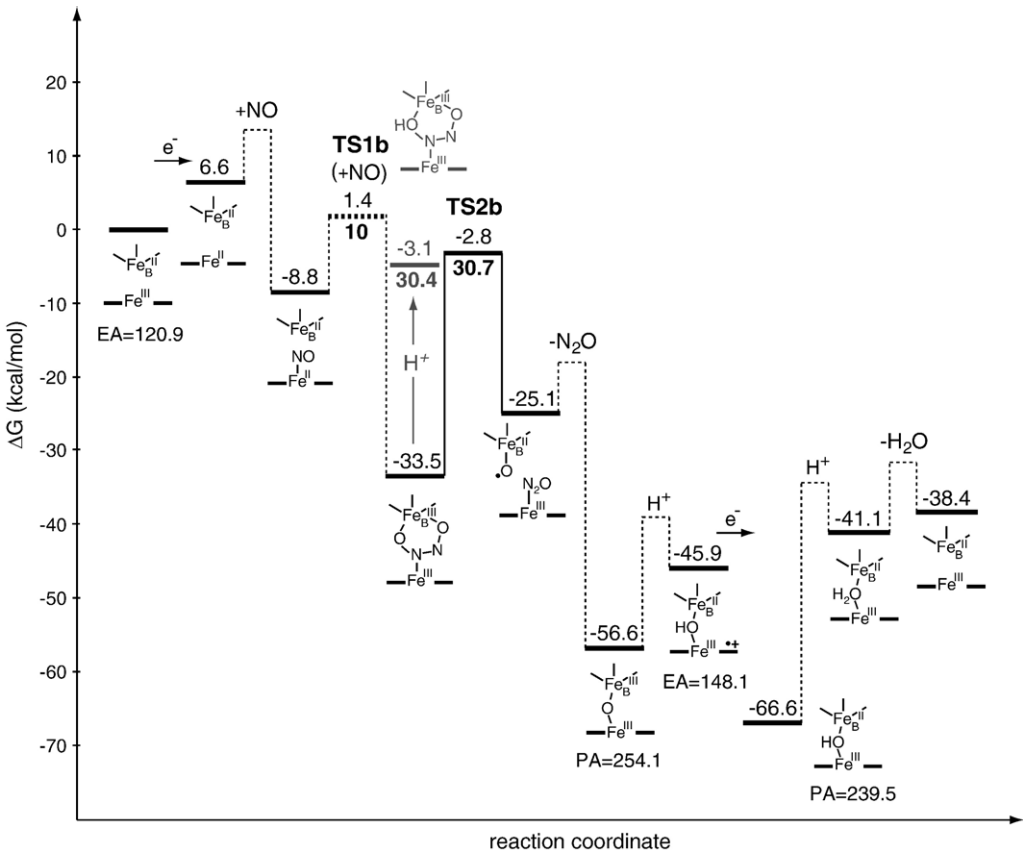

Fig. 9. Free energy profile of model B, tetrahedral Fe_B.

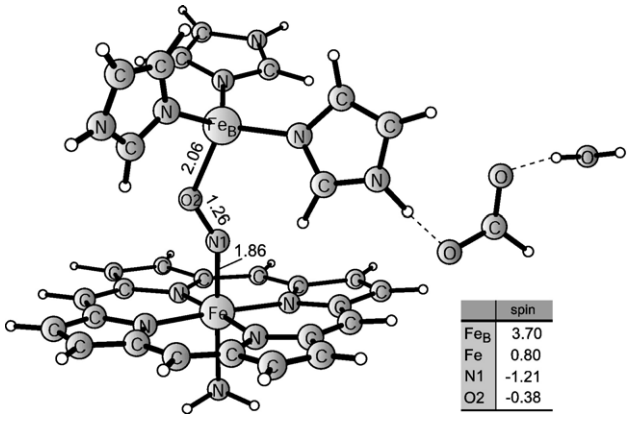

Fig. 10. Nitric oxide coordinating to the ferrous heme b_3 in model B.

and furthermore the cost of protonating this residue has be evaluated. However, considering the low proton affinity of the hyponitrite, the *trans* mechanism is presumably unfavored compare to the *cis:*b_3 mechanism.

Another mechanism proposed is the *cis*:Fe_B mechanism in which both NOs coordinate to the non-heme iron. However, this is not possible in model A since only one coordination site on Fe_B is empty. Furthermore, the affinity for NO is higher for heme b_3 than for Fe_B as discussed above. An additional reaction path, presumably giving the same intermediate as the *cis*:Fe_B mechanism, would be if NO binds to Fe_B and reacts in a similar way compared to TS1a described above. Then a reversed hyponitrite dianion intermediate would be formed with N1 coordinating to Fe_B and O2 to heme b_3. However, this structure is 12.5 kcal/mol less stable compared to the *cis:*b_3 structure seen in Fig. 6. Thus, the *cis:*b_3 mechanism is presumably favored compared to the alternative mechanisms.

4.3. Model B

In model B the non-heme iron has a tetrahedral coordination binding three histidines corresponding structurally to Cu_B in cytochrome oxidases, as discussed above (Section 2). The resulting free energy profile of the reduction of NO in model B is shown in Fig. 9.

4.3.1. Binding of NO

Similar to model A (Section 4.2), the first step in the reaction is assumed to be a reduction of the ferric heme b_3. The endergonic electron transfer is followed by the binding of NO which is exergonic by 8.6 kcal/mol compared to the heme b_3–Fe(III) Fe_B (II) intermediate. Thus, the affinity for nitric oxide in the fully reduced binuclear center is 12.3 kcal/mol higher in model B than in model A. NO binding to the ferrous heme b_3 induces an oxidation of the heme iron to almost a ferric state, reducing NO to a nitroxyl anion ($^3NO^-$) antiferromagnetically coupled to Fe_B and the oxidized heme b_3. The spin populations of the ferric heme b_3, N1 and O2 are 0.80, −1.21 and −0.38, respectively. Fe_B stays in its ferrous state and has a spin population of 3.70, see Fig. 10. The low coordination and neutral ligands of Fe_B makes it electron deficient, and therefore Fe_B is stabilized by the negatively charged nitroxyl anion. The stabilization of Fe_B when binding NO explains why the affnity for nitric oxide is higher in model B than in model A. Furthermore, in model B the bond strength of NO to Fe_B is almost as high as to heme b_3. However, in the case when NO coordinates with its nitrogen to Fe_B the intermediates formed by reacting with a second NO is clearly unfavored as will be shortly discussed below.

4.3.2. Formation of the N − N bond

The second nitric oxide enters the active site and forms an N − N bond without any enthalpy barrier. The free energy barrier for this reaction step therefore corresponds to the loss in translational entropy bringing NO to the transition state, i.e. approximately 10 kcal/mol. Since TS1b has a pure entropy barrier, it will depend on the concentration of NO, and 10 kcal/mol can therefore be viewed as the maximum barrier for this reaction step. It should be noted that similar to model A (Section 4.2), there is a spin flip on approaching TS1b. This spin flip of the NO coordinated between the two irons results in an antiferromagnetic coupling between heme b_3 and Fe_B and a ferromagnetic coupling between NO and Fe_B. The change in spin lowers the energy of the hyponitrite dianion intermediate formed in this step.

In model B the hyponitrite dianion intermediate can coordinate with both oxygens to the non-heme iron due to the unsaturated coordination of Fe_B. Therefore, the hyponitrite dianion intermediate is substantially stabilized, and the reaction step is exergonic by 24.7 kcal/mol relative to the heme b_3 nitrosyl complex and a free nitric oxide. Both irons are oxidized with spin populations of −1.08 and 4.13 on heme b_3 and Fe_B, respectively. The hyponitrite dianion forms a five-membered ring with Fe_B. The oxygens coordinating to the non-heme iron have spin population of 0.22 and 0.23, see Fig. 11 for distances and spin populations. In model B the *cis:*b_3 type of structure of the hyponitrite dianion is favored by > 20 kcal/mol compared to the corresponding *trans* and *cis:*Fe_B structures, making those mechanisms unlikely.

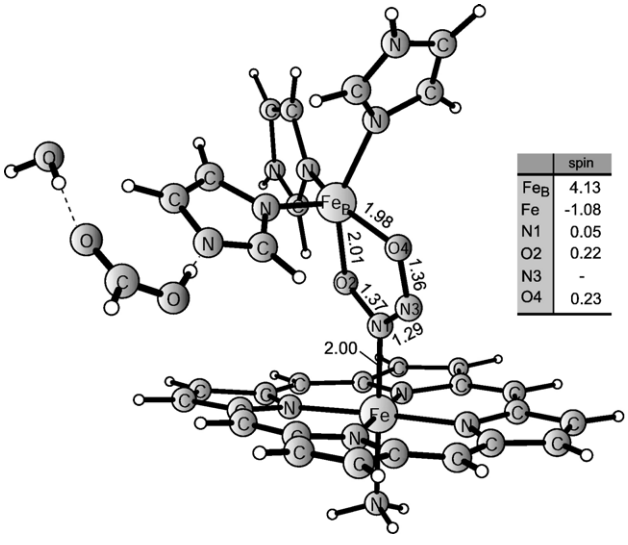

Fig. 11. The hyponitrite dianion intermediate coordinating between a ferric heme-b_3 and Fe_B in model B.

4.3.3. Cleaving an N − O bond forming N_2O

In the next reaction step one N − O bond should be cleaved, forming nitrous oxide and a Fe_B (IV)═O (Fig. 12). However, cleaving the N − O bond has a barrier of 30.7 kcal/mol, which is too high for the reaction to proceed via this mechanism. In a previous study the reduction of NO in a *ba*$_3$-type cytochrome oxidase was investigated. A protonation of the hyponitrite dianion, on the oxygen corresponding to O2 in the present study, was found to be necessary to cleave the N − O bond forming a hydroxyl group coordinating to Cu_B (II) [31]. A similar mechanism was investigated for model B in the present study. However, the proton affnity for the hyponitrite dianion intermediate is only 234.5 kcal/mol to be compared to PA^B_{bulk} = 264.8 kcal/mol. Thus, the protonation of the hyponitrite dianion forming hyponitrite would be endergonic by 30.4 kcal/mol. Even if the barrier for cleaving the N − O bond is decreased, the cost of the protonation is too high and the reaction would not go via this path.

Even though the barrier of TS2b was found to be too high, the remaining part of the reaction mechanism, corresponding to the one investigated for model A, was investigated to complete the picture of the reduction of NO in model B.

After the N − O bond is cleaved, nitrous oxide is coordinated to a ferric heme, and not to a ferrous one as in model A. Furthermore, the non-heme iron is not in the ferrylic state as in model A but rather a ferrous iron coordinating an oxyl radical. This is due to the coordination of Fe_B, which cannot stabilize highly oxidized states. This reaction step is endergonic by 8.4 kcal/mol relative to the hyponitrite dianion intermediate. Thus, the intermediate formed is quite unstable, and will decay fast by expelling the nitrous oxide forming a μ-oxo bridged diferric binuclear center, see Fig. 13. The μ-oxo bridge formed is 23.1 kcal/mol more stable than the hyponitrite dianion, see Fig. 9.

4.3.4. Reduction of the μ-oxo bridge to water

To complete the catalytic cycle the diferric μ-oxo bridge has to be reduced back to the mixed valence binuclear center while forming water. In this process, the remaining electron and two protons are transferred to the active site. In Section 4.1, the electron and proton affinities were parametrized to experimental reduction potentials giving an $EA^B_{heme\ b}$=127.5 kcal/mol and PA^B_{bulk}=264.8 kcal/mol, respectively. These reference values are used together with the calculated proton and electron affinities of the different intermediates, to evaluate the energetics of the reduction of the μ-oxo bridge to water, which is shown in Fig. 9.

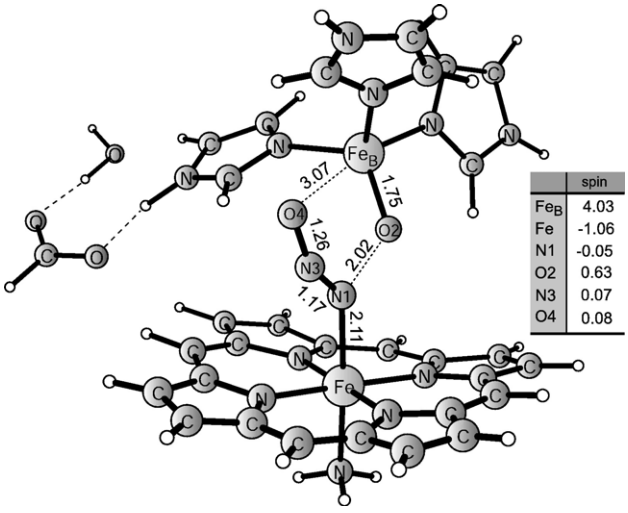

Fig. 12. TS2b, cleaving the N − O bond forming an oxyl radical coordinated to a ferrous Fe_B and a nitrous oxide coordinating to a ferric heme b_3.

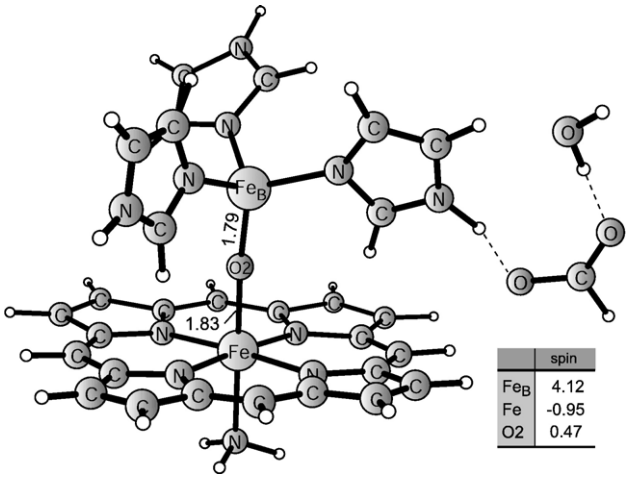

Fig. 13. Ferric heme b_3 and Fe_B bridged by a α-oxo group.

In addition to the high barrier for cleaving the N − O bond (TS2b), regeneration of the empty mixed valence binuclear center by reducing the μ-oxo bridge to water contains a large energy barrier of 28.2 kcal/mol, see Fig. 9. The high barrier is caused by the formation of a too stable hydroxyl group coordinating between the ferric heme b_3 and ferrous Fe_B, which results in a very endergonic protonation step forming water.

Experimentally the resting state of the oxidized NOR has been proposed to be a μ-oxo bridge, which is also the case in model B, see Fig. 9. Furthermore, as mentioned above in Section 4.2.4, the experimental reduction potentials for Fe_B measured at different pH correspond to the formation of either a hydroxyl group or water, coordinating between the ferric heme b_3 and ferrous Fe_B. Thus, depending on the protonation state of the solvent bridge the reduction of Fe_B is endergonic by 2.4 (OH) and 0.5 (H_2O) kcal/mol relative to the μ-oxo bridge, respectively [5,40]. In model B the corresponding processes are exergonic by 10.0 kcal/mol (OH) and endergonic by 15.5 (H_2O) kcal/mol, respectively. Thus, the deviations from the experiments are 12.0 and 16.0 kcal/mol for the formation of the hydroxyl group and water, respectively. These values can be compared to the corresponding deviations in model A, 8.1 and 1.3 kcal/mol, respectively, which shows that the reduction potentials of Fe_B are much better described in model A than in model B.

It can be concluded that model B has severe problems catalyzing the reduction of nitric oxide. The electron poor Fe_B coordination makes both the hyponitrite dianion and the bridging intermediates too stable. The stability of these

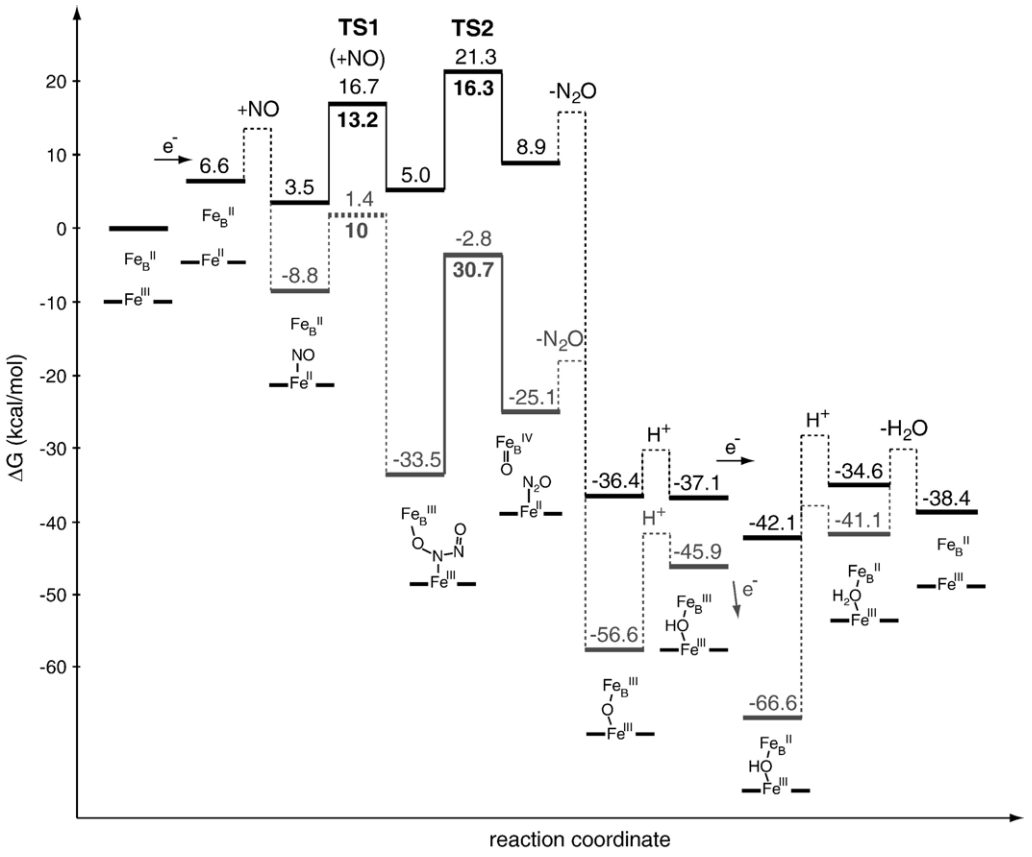

Fig. 14. Summary of the energy profiles of model A and B.

intermediates results in large energy penalties for both cleaving the N − O bond and the regeneration of the empty mixed valence binuclear site by reducing the μ-oxo bridge and expelling the water formed.

5. Conclusions

In the present study, the reduction mechanisms of two nitric oxides to nitrous oxide and water have been studied in two models of the binuclear site of nitric oxide reductase. Model A has an octahedral coordination of the non-heme Fe_B (3His–1Glu–H_2O) whereas model B has a tetrahedral coordination (3His) with the Glu and water being second shell ligands, see Fig. 2. The two models differ only in the arrangement of the ligands surrounding Fe_B, whereas heme b_3 is described identically, giving the same total charge for both models. The calculated free energy surfaces of the NO reduction in model A and B are summarized in Fig. 14. Both models follow the so-called *cis:*b_3 type of reaction mechanism where the reaction occurs on the heme b_3 iron. This type of mechanism allows the donation of one electron from each iron and stabilizes the $N_2ON_2^{2-}$ species formed.

In model A, the first half of the reaction, forming the ferrylic Fe_B and nitrous oxide coordinating to the ferrous heme b_3, is an endergonic process. However, as discussed above in Section 4.2.1, the binding energy of NO to ferrous heme has been shown to be underestimated by 7–8 kcal/mol in cytochrome oxidase. If the bond strength for NO is assumed to be under-estimated to a similar extent in NOR, a correction to the free energy surface for model A (Fig. 14) would make the nitrosyl intermediate the resting state instead of the empty mixed valence binuclear center.

Cleaving an N − O bond in the hyponitrite dianion intermediate has an intrinsic barrier of 16.3 kcal/mol. This is in good agreement with the experimental turnover rate (~1400 mol NO mol enz^{-1} min^{-1} [38]) corresponding to a rate determining barrier of 15.9 kcal/mol. However, as can be seen in Fig. 14, the barrier is 21.3 kcal/mol compared to the empty mixed valence binuclear center, since both the binding of NO and the formation of the hyponitrite dianion intermediate are slightly endergonic. With consideration of the uncertainty in the modeling of the coordination of Fe_B in the present study, the agreement is satisfactory. In the next reaction step, the very exergonic formation of the μ-oxo bridge between the two ferric irons drives the reaction forward. Reducing and protonating the μ-oxo bridge and expelling the water formed from the active site are fairly thermoneutral processes, in agreement with experiments. Thus, most energy is released in the formation of the μ-oxo bridge.

Model B, on the other hand, has a tetrahedral coordination of Fe_B corresponding to the structure obtained when fitting the primary sequence of NorB in *P. stutzeri* to the cytochrome *c* oxidase structure in *Pa. denitrificans* [9]. The tetrahedral coordination was shown to stabilize both the hyponitrite dianion and O(H)-bridged intermediates too much, which results in a too high barrier for cleaving the N − O bond (TS2b) and also a too endergonic reduction of the hydroxyl group coordinating in between the ferric heme b_3 and ferrous Fe_B forming water, see Fig. 14.

The non-heme iron in the binuclear center of NOR thus seems to need a negatively charged ligand and has most likely an octahedral coordination. Even though the coordination does not have to correspond exactly to the one in model A, the energetics is not believed to change much if the glutamate is exchanged for, e.g., a hydroxyl group. Neither should an exchange of His207 for a solvent molecule, forming the 2His–1Glu motif, common in other non-heme mononuclear enzymes, have any major effects on the energetics. The most critical steps in the proposed reaction mechanism are the formation of the hyponitrite dianion and the formation of the ferrylic Fe_B. The coordination of the non-heme iron should avoid forming a too stable hyponitrite dianion intermediate which would lead to an increased barrier for the N − O bond cleavage. The formation of $N_2ON_2^{2-}$ should ideally be close to thermoneutral. Furthermore, Fe_B must have a relatively stable ferrylic state, and can therefore not have an electron deficient surrounding. Since the non-heme iron with a 2His–1Glu motif has been shown to be able to be oxidized to Fe(IV)═O in other mononuclear non-heme iron enzymes [41,42] it seems likely that it could work also in NOR. Simultaneously with cleaving an N − O bond and forming the ferrylic Fe_B, a stable nitrous oxide is formed, which makes the reaction energetically feasible.

In a previous study, the reduction mechanism of nitric oxide in a cytochrome oxidase was investigated. In that case, the intermediate corresponding to the ferrylic Fe_B in the present mechanism would be Cu_B (III)═O, which is not energetically feasible, and the hyponitrite dianion has to be protonated to cleave the N − O bond [31]. A mechanism for the NO reduction in which a ferrylic Fe_B is formed could be one reason for having an iron as the non-heme metal ion in NOR and not Cu as in cytochrome oxidase.

Analyzing the models of the NOR structure it can be difficult to understand how a glutamate could coordinate to Fe_B, even though Glu211 and Glu280 are located in the vicinity. One possibility could be that the α-helix VI incorporating His207 and Glu211 is shifted upward approximately one turn compared to the modeled structure. His207 would then be exchanged as an Fe_B ligand for Glu211 which would explain why this glutamate is essential for activity. One way of testing this possibility would be to mutate His207. If the latter is not an Fe_B ligand it should most likely have a small effect on the enzyme activity. Another possibility, as mentioned above, is the coordination of a hydroxyl group and a water molecule in addition to the three conserved histidines forming an octahedral coordination around Fe_B. The hydroxyl group would in this case play the role of the glutamate as a negatively charged ligand, which in the present study seems very important for the reduction of NO.

In conclusion, a tetrahedral non-heme iron is most likely not feasible for the coordination of Fe_B. Instead an octahedral coordination with one negatively charged ligand in the first coordination shell gives energetics in quite good agreement with what has been experimentally observed.

Appendix A. Supplementary data

Supplementary data associated with this article can be found, in the online version, at doi:10.1016/j.bbabio.2006.04.008.

References

[1] A.M. Gardner, R.A. Helmick, P.R. Gardner, Flavorubredoxin, an inducible catalyst for nitric oxide reduction and detoxification in *Escherichia coli*, J. Biol. Chem. 277 (2002) 8172–8177.

[2] K. Nakahara, T. Tanimoto, K. Hatano, K. Usuda, H. Shoun, Cytochrome p-450 55a1 (p-450dnir) acts as nitric oxide reductase employing NADH as the direct electron donor, J. Biol. Chem. 268 (1993) 8350–8355.

[3] M.R. Cheesman, W.G. Zumft, A.J. Thomson, The mcd and epr of the heme centers of nitric oxide reductase from *Pseudomonas stutzeri*: evidence that the enzyme is structurally related to the heme-copper oxidases, Biochemistry 37 (1998) 3994–4000.

[4] P. Girsch, S. de Vries, Purification and initial kinetic and spectroscopic characterization of no reductase from *Paracoccus denitrificans*, Biochim. Biophys. Acta 1318 (1997) 202–216.

[5] K.L.C. Grönberg, M.D. Roldán, L. Prior, G. Butland, M.R. Cheesman, D.J. Richardson, S. Spiro, A.J. Thomson, N.J. Watmough, A low-redox potential heme in the dinuclear center of bacterial nitric oxide reductase: implications for the evolution of energy-conserving heme-copper oxidases, Biochemistry 38 (1999) 13780–13786.

[6] J. Hendriks, U. Gohlke, M. Saraste, From no to oo: nitric oxide and dioxygen in bacterial respiration, J. Bioenerg. Biomembr. 30 (1998) 15–24.

[7] N. Sakurai, T. Sakurai, Isolation and characterization of nitric oxide reductase from *Paracoccus halodenitrificans*, Biochemistry 36 (1997) 13809–13815.

[8] J. Hendriks, A. Warne, U. Gohlke, T. Halita, C. Ludovici, M. Lübben, M. Saraste, The active site of the bacterial nitric oxide reductase is a dinuclear iron center, Biochemistry 37 (1998) 13102–13109.

[9] W.G. Zumft, Nitric oxide reductases of prokaryotes with emphasis on the respiratory heme- copper oxidase type, J. Inorg. Biochem. 99 (2005) 194–215.

[10] A. Kannt, H. Michel, M.R. Cheesman, A.J. Thomson, A.B. Dreusch, H. Körner, W.G. Zumft, G.W. Canters, E. Vijgenboom (Eds.), Biological electron transfer chains: genetics, composition and mode of operation, Kluwer Academic Publishers, Dordrecht, 1998.

[11] G. Butland, S. Spiro, N.J. Watmough, D.J. Richardson, Two conserved glutamates in the bacterial nitric oxide reductase are essential for activity but not assembly of the enzyme, J. Bacteriol. 183 (2001) 189–199.

[12] J. Hendriks, A. Jasaitis, M. Saraste, M.I. Verkhovsky, Proton and electron pathways in the bacterial nitric oxide reductase, Biochemistry 41 (2002) 2331–2340.

[13] P. Moënne-Loccoz, S. de Vries, Structural characterization of the catalytic high-spin heme b of nitric oxide reductase: a resonance raman study, J. Am. Chem. Soc. 120 (1998) 5147–5152.

[14] L. Que Jr., One motif—Many different reactions, Nature Struc. Biol. 7 (2000) 182–184.

[15] L. Que Jr., R.Y.N. Ho, Dioxygen activation by enzymes with mononuclear non-heme iron active sites, Chem. Rev. 96 (1996) 2607–2624.

[16] R. Silaghi-Dumitrescu, D.M. Kurtz Jr., L.G. Ljungdahl, W.N. Lanzilotta, X-ray crystal structures of *Moorella thermoacetica* fpra. novel diiron site structure and mechanistic insights into scavenging nitric oxide reductase, Biochemistry 44 (2005) 6492–6501.

[17] R. Silaghi-Dumitrescu, E.D. Coulter, A. Das, L.G. Ljungdahl, G.N.L. Jameson, B.H. Huynh, D.M. Kurtz Jr., A flavodiiron protein and high molecular weight rubredoxin from moorellathermoacetica with nitric oxide reductase activity, Biochemistry 42 (2003) 2806–2815.

[18] A.D. Becke, Density-functional thermochemistry. iii. The role of exact exchange, J. Chem. Phys. 98 (1993) 5648–5652.

[19] C. Lee, W. Yang, R.G. Parr, Development of the colle-salvetti correlation-energy formula into a functional of the electron density, Phys. Rev. B. 37 (1988) 785–789.

[20] M.J. Frisch, G.W. Trucks, H.B. Schlegel, G.E. Scuseria, M.A. Robb, J.R. Cheeseman, J.J.A. Montgomery, T. Vreven, K.N. Kudin, J.C. Burant, J.M. Millam, S.S. Iyengar, J. Tomasi, V. Barone, B. Mennucci, M. Cossi, G. Scalmani, N. Rega, G.A. Petersson, H. Nakatsuji, M. Hada, K. Ehara, M.

Toyota, R. Fukuda, J. Hasegawa, M. Ishida, T. Nakajima, Y. Honda, O. Kitao, H. Nakai, M. Klene, X. Li, J.E. Knox, H.P. Hratchian, J.B. Cross, C. Adamo, J. Jaramillo, R. Gomperts, R.E. Stratmann, O. Yazyev, A.J. Austin, R. Cammi, C. Pomelli, J.W. Ochterski, P.Y. Ayala, K. Morokuma, G.A. Voth, P. Salvador, J.J. Dannenberg, V.G. Zakrzewski, S. Dapprich, A.D. Daniels, M.C. Strain, O. Farkas, D.K. Malick, A.D. Rabuck, K. Raghavachari, J.B. Foresman, J.V. Ortiz, Q. Cui, A.G. Baboul, S. Clifford, J. Cioslowski, B.B. Stefanov, G. Liu, A. Liashenko, P. Piskorz, I. Komaromi, R.L. Martin, D.J. Fox, T. Keith, M.A. Al-Laham, C.Y. Peng, A. Nanayakkara, M. Challacombe, W. Gill, B. Johnson, W. Chen, M.W. Wong, C. Gonzalez, J.A. Pople, Gaussian 03, Revision B.03, Gaussian Inc., Pittsburgh, PA, 2003.

[21] Schrodinger, LLC, Portland, Oregon, Jaguar 5.5 (2003).

[22] L.M. Blomberg, M.R.A. Blomberg, P.E.M. Siegbahn, A theoretical study of myoglobin working as a nitric oxide scavenger, J. Biol. Inorg. Chem. 9 (2004) 923–935.

[23] L.M. Blomberg, M.R.A. Blomberg, P.E.M. Siegbahn, W.A. van der Donk, A.L. Tsai, A quantum chemical study of the synthesis of prostaglandin g2 by the cyclooxygenase active site in prostaglandin endoperoxide h synthase 1, J. Phys. Chem., B. 107 (2003) 3297–3308.

[24] D.J. Tannor, B. Marten, R. Murphy, R.A. Friesner, D. Sitkoff, A. Nicholls, M. Ringnalda, W.A. Goddard III, B. Honig, Accurate first principles calculation of molecular charge distributions and solvation energies from ab initio quantum mechanics and continuum dielectric theory, J. Am. Chem. Soc. 116 (1994) 11875–11882.

[25] M.R.A. Blomberg, P.E.M. Siegbahn, G.T. Babcock, Modeling electron transfer in biochemistry: a quantum chemical study of charge separation in *Rhodobacter sphaeroides* and photosystem ii, J. Am. Chem. Soc. 120 (1998) 8812–8824.

[26] D.M. Popović, J. Quenneville, A.A. Stuchebrukhov, Dft/electrostatic calculations of pK_a values in cytochrome *c* oxidase, J. Phys. Chem., B. 109 (2005) 3616–3626.

[27] L.A. Curtiss, K. Raghavachari, R.C. Redfern, J.A. Pople, Assessment of gaussian-3 and density functional theories for a larger experimental test set, J. Chem. Phys. 112 (2000) 7374–7383.

[28] P.E.M. Siegbahn, M.R.A. Blomberg, Density functional theory of biologically relevant metal centers, Annu. Rev. Phys. Chem. 50 (1999) 221–249.

[29] P.E.M. Siegbahn, M.R.A. Blomberg, Transition-metal systems in biochemistry studied by high-accuracy quantum chemical methods, Chem. Rev. 100 (2000) 421–437.

[30] M.R.A. Blomberg, P.E.M. Siegbahn, A quantum chemical approach to the study of reaction mechanisms of redox-active metalloenzymes, J. Phys. Chem., B. 105 (2001) 9375–9386.

[31] L.M. Blomberg, M.R.A. Blomberg, P.E.M. Siegbahn, A theoretical study on nitric oxide reductase activity in a ba_3-type heme-copper oxidase, Biochim. Biophys. Acta 1757 (2006) 31–46.

[32] E. Pinakoulaki, S. Gemeinhardt, M. Saraste, C. Varotsis, Nitric-oxide reductase structure and properties of the catalytic site from resonance raman scattering, J. Biol. Chem. 277 (2002) 23407–23413.

[33] L.M. Blomberg, M.R.A. Blomberg, P.E.M. Siegbahn, A theoretical study on the binding of o_2, no and co to heme proteins, J. Inorg. Biochem. 99 (2005) 949–958.

[34] H. Kumita, K. Matsuura, T. Hino, S. Takahashi, H. Hori, Y. Fukumori, I. Morishima, Y. Shiro, No reduction by nitric-oxide reductase from denitrifying bacterium *Pseudomonas aeruginosa*, J. Biol. Chem. 279 (2004) 55247–55254.

[35] V. Shafirovich, S.V. Lymar, Nitroxyl and its anion in aqueous solutions: spin states, protic equilibria, and reactivities toward oxygen and nitric oxide, Proc. Natl. Acad. Sci. U. S. A. 99 (2002) 7340–7345.

[36] A. Bassan, M.R.A. Blomberg, P.E.M. Siegbahn, Mechanism of aromatic hydroxylation by an activated fe^{IV}═o core in tetrahydrobiopterin-dependent hydroxylases, Chem. Eur. J. 9 (2003) 4055–4067.

[37] A. Bassan, M.R.A. Blomberg, P.E.M. Siegbahn, Mechanism of dioxygen cleavage in tetrahydrobiopterin-dependent amino acid hydroxylases, Chem. Eur. J. 7 (2003) 106–115.

[38] E. Forte, A. Urbani, M. Saraste, P. Sarti, M. Brunori, A. Giuffrè, The cytochrome *c*bb_3 from *Pseudomonas stutzeri* displays nitric oxide reductase activity, Eur. J. Biochem. 268 (2001) 6486–6490.

[39] P. Moënne-Loccoz, O.-M.H. Richter, H.-w. Huang, I.M. Wasser, R.A. Ghiladi, K.D. Karlin, S. de Vries, Nitric oxide reductase from *Paracoccus denitrificans* contains an oxo-bridged heme/non-heme diiron center, J. Am. Chem. Soc. 122 (2000) 9344–9345.

[40] S.J. Field, L. Prior, M.D. Roldán, M.R. Cheesman, A.J. Thomson, S. Spiro, J.N. Butt, N.J. Watmough, D.J. Richardson, Spectral properties of bacterial nitric-oxide reductase, J. Biol. Chem. 277 (2002) 20146–20150.

[41] J.C. Price, E.W. Barr, B. Tirupati, J.M. Bollinger Jr., C. Krebs, The first direct characterization of a high-valent iron intermediate in the reaction of an α-ketoglutarate-dependent dioxygenase: A high-spin fe(iv) complex in taurine/α-ketoglutarate dioxygenase (taud) from *Escherichia coli*, Biochemistry 42 (2003) 7497–7508.

[42] P.M. Riggs-Gelasco, J.C. Price, R.B. Guyer, J.H. Brehm, E.W. Barr, J.M. Bollinger Jr., C. Krebs, Exafs spectroscopic evidence for an fe═o unit in the fe(iv) intermediate observed during oxygen activation by taurine:α-ketoglutarate dioxygenase, J. Am. Chem. Soc. 126 (2004) 8108–8109.